Palaeogeography, Palaeoclimatology, Palaeoecology 571 (2021) 110387

Contents lists available at ScienceDirect

Palaeogeography, Palaeoclimatology, Palaeoecology

journal homepage: www.elsevier.com/locate/palaeo

Invited research papers

Reconstruction of the Holocene sedimentary–ecological complex in the incised valley of the Yangtze Delta, China

Feng Jiang [a,b], Yanna Wang [a,*], Xiaoshuang Zhao [a], Yan Liu [a], Jing Chen [a], Qianli Sun [a], Maotian Li [a], Brian Finlayson [c], Zhongyuan Chen [a]

[a] State Key Laboratory of Estuarine and Coastal Research, East China Normal University, Shanghai 200062, China
[b] State Key Laboratory of Marine Geology, Tongji University, Shanghai 200092, China
[c] School of Geography, The University of Melbourne, Victoria 3010, Australia

ARTICLE INFO

Editor: Thomas Algeo

Keywords:
Holocene strata
Sr/Ba
Foraminifera–diatom spectra
Anaerobic bottom–water
Sedimentation rate
Sea-level rise

ABSTRACT

The well-^{14}C–dated sediment core HM retrieved from the Yangtze River mouth was used to reconstruct the Holocene sedimentary–ecological complex of its incised valley. The complete Holocene sedimentary facies that were exclusively formed in the valley and evidenced by bio-geochemical measurement, showed the Latest Pleistocene fluvial facies to the Early-Holocene marine facies, and the Middle-Late Holocene deltaic facies. The established Holocene stratigraphic framework consists of 3 (I-III) infilling phases, of which phase I demonstrated the most rapidly infilling with coastal sediments into the valley (1.0 cm/yr), driven by the Early Holocene marine transgression. The remarkably low sedimentation rate of 0.1 cm/yr of phase II to the relatively low rate of 0.7 cm/yr of phase III occurred during the Middle-Late Holocene, reflecting sediments transported from river basin to directly fill in the valley along with deltaic depocenter shifted seawards as retrogressive processes. In addition, our microfossil (foraminifera and diatom) spectra displayed 3 distinctive biological stages with related sedimentary–ecological implications. During the Early Holocene, there were remarkably high numbers of diatom communities but few foraminifera, then followed a zone of less abundant microfossils between ca. 9.0–5.0 ka. After this time, richer foraminiferal communities appeared but diatoms were less abundant. The massive sediment infilling in the Early Holocene in the deeper (>60 m) incised valley would suppress benthic foraminiferal development, most likely due to anaerobic conditions in the lower water column. However, the flourishing diatom communities persisted in the brackish marine water associated with sea-level rise. The zone with fewer microfossils corresponded generally with the Middle Holocene sandy ridge formation at the core site, leading to poorer bio–preservation. After ca. 5.0 ka, foraminiferal communities gradually became adapted to the reduced salinity of the estuarine water associated with the deltaic progradation, though this appears not to have supported the diatom communities.

1. Introduction

The incised valleys on delta coasts of Late Pleistocene age are elongated V–shaped topographic lowlands opening seawards (Dalrymple et al., 1994; Zaitlin et al., 1994). These valleys served as the main gateway for sediment transport from the river basin to the continental shelf when global sea level was ca. 120–150 m lower during the Latest Glacial Maximum (LGM) (Pluet and Pirazzoli, 1991). They were subsequently filled by sediment deposited during the Holocene sea-level rise (Dalrymple et al., 1992; Blum et al., 2013). The thick Holocene sediments (often >60–80 m) that are accumulated in these incised valleys, form a special sedimentary archive for paleo–environmental reconstruction (Boyd et al., 2006). Previous studies have shown that detailed information on paleoenvironmental changes including climate change, sea level fluctuation, sediment transport, and morphodynamic responses to river and coastal hydrodynamics can be deciphered from the sediments preserved this way (Dalrymple et al., 1994).

This sediment infilling model can be observed in many incised valleys across the world (Tanabe et al., 2006; Chaumillon et al., 2010; Tanabe et al., 2015; Clement and Fuller, 2018; Wang et al., 2020). A

* Corresponding author.
E-mail addresses: ynwang@sklec.ecnu.edu.cn (Y. Wang), xszhao@sklec.ecnu.edu.cn (X. Zhao), liuyan@sklec.ecnu.edu.cn (Y. Liu), jchen@geo.ecnu.edu.cn (J. Chen), qlsun@sklec.ecnu.edu.cn (Q. Sun), mtli@sklec.ecnu.edu.cn (M. Li), brianlf@unimelb.edu.au (B. Finlayson), z.chen@sklec.ecnu.edu.cn (Z. Chen).

https://doi.org/10.1016/j.palaeo.2021.110387
Received 2 December 2020; Received in revised form 26 March 2021; Accepted 27 March 2021
Available online 3 April 2021

citable example can be seen in the incised valley of the Mekong River Delta. The Late Pleistocene fluvial sediment was deposited in the valley ca. 13.0–9.5 ka when sea level was far lower than the present. There occurred a rapid flooding sedimentation on shelf between 9.5 and 8.5 ka before the valley was inundated. The valley was completely infilled with deltaic sediments after ca.7.5 ka, when the sea-level rise began to decelerate leading to deltaic deposition (Ta et al., 2005; Tjallingii et al., 2010). Other similar examples are the deltas of Mississippi (Greene et al., 2007) and Nile (Pennington et al., 2017). However, there are spatiotemporal variability among these incised valleys due to different geographic backgrounds. These relate to regional tectonic subsidence, continental margin type, basin physiography, catchment geology, river basin size and coastal hydrodynamics (Wang et al., 2020). The river-basin scale exerts control over the rates of sediment supply and sediment accommodation in the valley, and the geometry of the continental shelf can affect the timing of the invasion of the sea into the valley. In particular, basin–scale hydroclimate (precipitation, discharge and sediment flux) can make individual incised valleys environmentally distinctive (Wang et al., 2020).

The incised valley of the Yangtze Delta, as it enters the East China Sea, is an immense sediment sink. There has been considerable research conducted on this, including the Holocene stratigraphy and sedimentary facies, the morphodynamical processes, and environmental evolution in relation to sea-level rise (Chen and Stanley, 1998; Li et al., 2002; Hori et al., 2001, 2002). Hori et al. (2001) have established the Late Quaternary stratigraphic framework in the Yangtze incised valley, focusing on high-resolution-dated sedimentary facies of sediment boreholes. Li et al. (2002) built a sediment infilling model of the valley, emphasizing stratigraphic framework and environmental evolution. A recent study by Song et al. (2013) presented the earliest tidal shoal formed in the delta apex relating to the maximal Holocene marine transgression.

It is worthy here to reiterate that our previous study (Jiang et al., 2020) has reported the sedimentary processes of the Yangtze incised valley, revealing the depocenter shift under the control of coastal hydrodynamics, especially driven by the Coriolis Force. In the study, we are to narrate that although there were extensive researches conducted on incised valleys in the world, including the Yangtze Delta, most appeared to focus on sedimentological aspects and associated sediment dynamics, only a few on sedimentary–ecological combination. In Jiang et al. (2020), we also reported that foraminiferal distribution is unexpectedly low or absent in the Early-Middle Holocene sediment of the incised valley, being reversal to strong marine transgression at the time. This has left a knowledge gap in the understanding of such large incised valley across broader scale of paleo-ecological conditions.

Therefore, the present study attempts the reconstruction of the incised valley of the Yangtze Delta in a sedimentary–ecological setting, using integrated sediment and microfossil (foraminifera and diatom) proxies. The primary research goal is that we will continue to refine the Holocene environmental change of the valley by adding newly measured bio-geochemical sediment proxies, and on this base, the profound analysis of microfossil occurrence and bio-dynamics is used to reconstruct the sedimentary-ecological conditions of the valley. The results will complement the former study of the incised valley, and shall shed light on any analogues in future research.

2. Physical setting

The Yangtze Delta is one of the largest fluvially-tidally dominated deltas in the world, occupying an area > 20,000 km^2 (exclusive of the subaqueous part). Zhenjiang, the last gorge on the lower Yangtze, ca. 250 km inland from the present–day river mouth, is the delta apex (Fig. 1A). In a broader topographic context, the delta can be divided into the paleo–incised valley, where the present main river channel enters the estuary, and the extensive northern and southern delta plains (Yan and Xu, 1987; Li et al., 2000, 2002).

The pre–Holocene incised valley is ca. 15 km wide at the delta apex and ca. 120 km wide at the river mouth (Fig. 1A,B). The valley was 50–70 m below the present mean sea–level (MSL) (Li et al., 2002; Jiang et al., 2020). Topographically, the V–shaped incised valley is delineated by both the pre–Holocene coastal flanks (Fig. 1B). To the south it is flanked by a huge promontory, ca. 5–50 m below MSL, while to the north there is flat coastland, ca. 20 m below MSL (Fig. 1B). The incised valley was buried by thicker (>60 m) Holocene sediments, including 20–30 m of Early Holocene sediment. This contrasts with both the coastal flanks where such sedimentation seldom occurred due to the raised pre–Holocene topography (Jiang et al., 2020).

An extensive tidal flat occurs on the present coastal fringe, serving as an important ecological buffer zone. Three large islands, Chongming, Changxing and Hengsha (Fig. 1A) have developed since the Late Holocene in the river mouth area, part of the infilling of the incised valley. The delta plain is a watery lowland, elevated 3–5 m above MSL. The *meso*–tidal range on the coast is 2.6 m, on average, but >4.0 m during seasonal peaks (Chen et al., 1988). The study area has a monsoonal climate, with an average temperature of 17.6 °C and average precipitation of 1100 mm/yr, with 70% falling in summer.

3. Materials and methods

3.1. Sediment coring

The sediment core HM was drilled in the Yangtze River mouth area (Fig. 1A), using a 9 cm diameter rotary coring tube. Core HM (121°5.56′ N, 31°57.42′ E) is 3.4 m above MSL and 69.8 m deep. Core sediment was retrieved continuously via a one–meter drill with a 90% recovery rate. Details of sampling of core sediments refer Jiang et al. (2020).

3.2. Radiocarbon dating

In total, there were 16 samples collected from HM for radiocarbon dating, using Accelerator Mass Spectrometry (AMS) (details refer S_Table 1 and Jiang et al., 2020). The Bacon age–depth model was applied using a linear interpolator with Bacon Modeling Software 2.2 (Blaauw and Christen, 2011). A median age was determined for each date from its 2σ calibrated age distribution. The dates reported in this text simply as ka are, strictly speaking, calibrated years before present – cal. yr BP.

3.3. Grain size test

Sixty–nine (69) core samples were taken for grain size analysis from core HM (S_Table 2). Grain size was measured using a Beckman Coulter LS13 320 Particle Size Analyser. About 0.1 g of pre–homogenized sediment was pretreated with 30% H_2O_2 to oxidize organic matter and HCl (10%) solution to remove carbonates, after which the sample was dispersed and homogenized using sodium hexametaphosphate solution and ultrasonic approaches.

3.4. Strontium and barium test

The 64 samples from core HM were also analyzed for strontium (Sr) and barium (Ba) content and the results are given in S_Table 3. 1.5 g of dried sample was ground to powder in an agate mortar, placed in a 70 ml polyethylene centrifuge tube and 50 ml dilute acetic acid was added. After ultrasonic shaking for 1 h the supernatant liquid was collected and transferred to an evaporating dish. The sample was heated until all liquid was evaporated. The evaporation residue was dissolved in 50 ml dilute nitric acid solution. The Sr and Ba taken into solution was tested by Inductively Coupled Plasma Mass Spectrometry (ICP–MS). A modified method, Sr/Ba–HAc (Wang et al., 2019) for measuring Sr and Ba was applied in the present study.

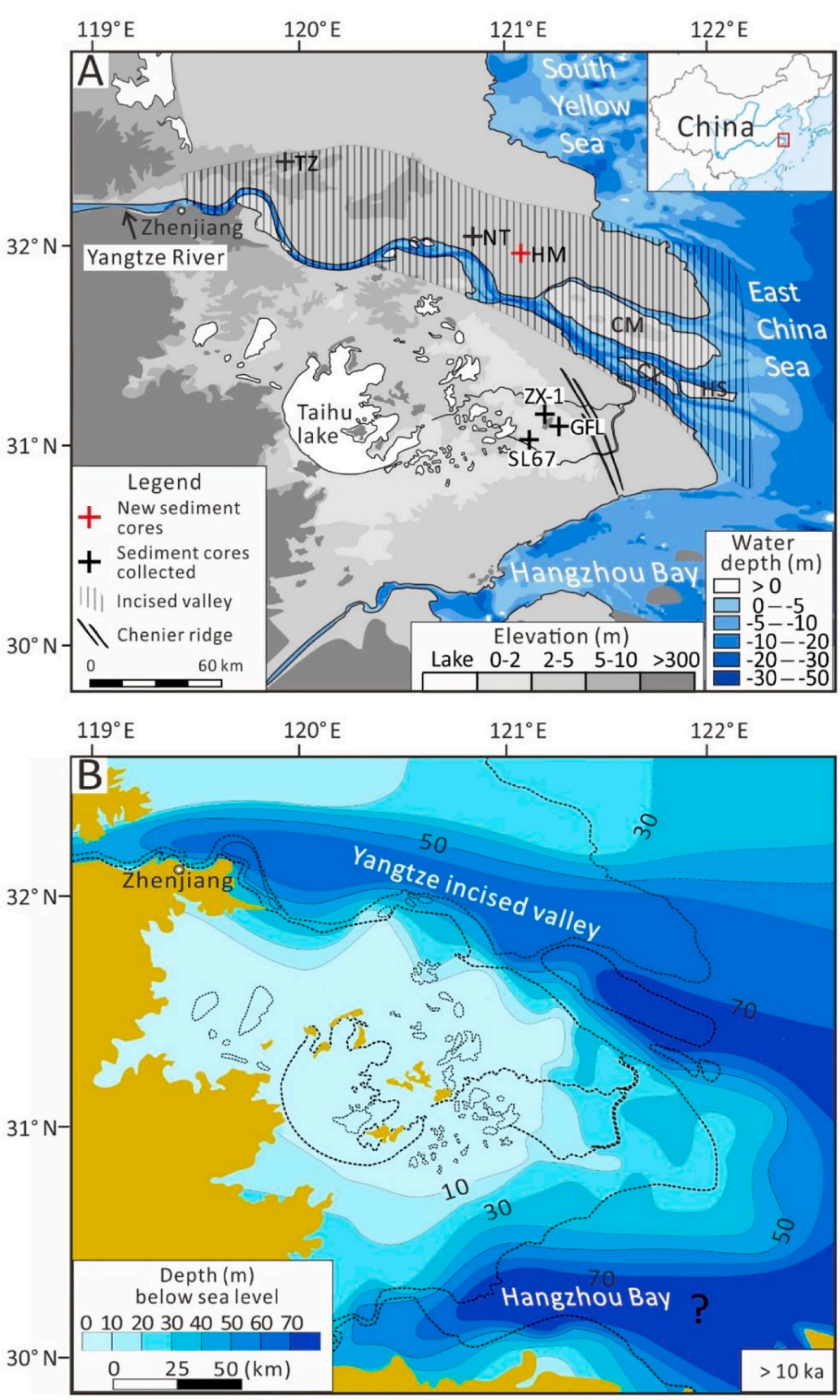

Fig. 1. A) Yangtze Delta, indicating the location of the sediment cores used in this study. CM – Chongming Island; HS – Hengsha Island; CX – Changxing Island. B) The pre–Holocene topography of the Yangtze Delta, including its incised valley (modified after Jiang et al., 2020).

3.5. Microfossils test

Microfossil analyses were performed on samples of core HM at a sampling interval of 1.5–2.0 m. Foraminifera and diatoms in this study were considered as two distinct microfossil communities and both flux and species were taken into account although foraminiferal distribution was preliminarily discussed in Jiang et al. (2020). 34 samples were collected for the analysis of foraminifera and 39 for the analysis of diatoms (S_Table 4 and S_Table 5).

One set of samples was passed through a 63 μm filter mesh to isolate the foraminiferal component. Foraminiferal identification followed the procedures of Wang et al. (1985) and Lei and Li (2016). In another set of samples, diatoms were isolated by the flotation method and identification followed the procedures in Renberg (1990) and Battarbee et al. (2001). Microfossils were identified and counted with a microscope at a magnification of 40× for foraminifera, and 400× and 1000× for diatoms.

D_{flux} represents the flux change of the two communities (grains/cells cm^{-2} yr^{-1}). The relative abundance for each taxon (D_{re}) was calculated as a percentage based on the grain/cell sums of each sample:

$$D_{re} = \frac{N_{sp}}{N} \times 100\% \quad (1)$$

where N_{sp} is the sum of one taxon in each sample and N is the total grains/cells counted for each sample.

The species diversity was evaluated using the species richness index D (Margalef, 1968):

$$D = (S-1) \times log_2(N) \quad (2)$$

where S is the number of species and N is the total grains/cells, counted for each sample.

Multiple statistical approaches were employed to detect significant ecological shifts in the microfossil communities. Before testing, only taxa with relative abundance >1% were selected for analysis, to minimize the impact of rare species on the result of significance tests. D_{re} matrix data of foraminifera and diatoms were analyzed by CONISS, using the Tilia software (Grimm, 1987) to identify ecological zonation in core HM. The diatom dataset was also analyzed using the two–way indicator species analysis TWINSPAN (Hill and Šmilauer, 2005) to distinguish the typical species in the assemblages. Foraminiferal assemblages were based on proportions of dominant species and related ecological characteristics.

4. Results

4.1. Holocene strata

The well-^{14}C-dated sediments of core HM, together with newly-measured bio-sedimentological data can be used to establish the Holocene strata in the incised valley, represented by 7 units (I–VII, core upward), shown in Fig. 2. Chronological time range of this study followed our previous study (Jiang et al., 2020), i.e. ca. 12–7 ka (Early-Holocene), ca. 7–4 ka (Middle-Holocene) and ca. 4–0 ka (Late-Holocene).

Unit I (69.8–63.8 m) consists of yellowish grey medium–fine sand

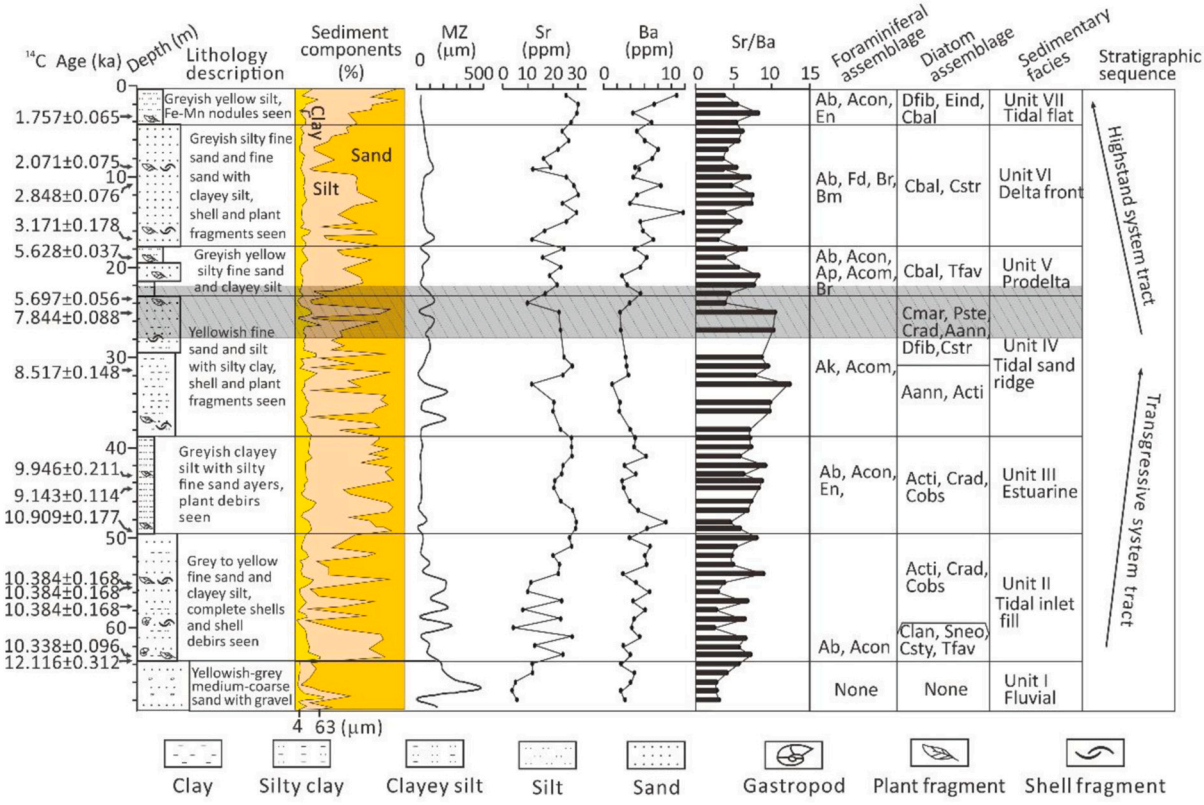

Fig. 2. Holocene strata in core HM and interpreted sedimentary facies, transgressive systems tract (TST) and highstand systems tract (HST) (modified after Jiang et al., 2020). Note, the zone in hashed grey (core HM) represents the low sedimentation period (ca. 8.5–4.5 ka based on the age–depth model in Fig. 3). Foraminiferal abbreviation: Ab – *Ammonia beccarii* vars.; Acon – *Ammonia convexidorsa*; En – *Epistominella naraensis*; Fd – *Florilus decorus*; Br – *Bolivina robusta*; Bm – *Bulimina marginata*; Ap – *Ammonia pauciloculata*; Acom – *Ammonia compressiuscula*; Ak – *Ammonia ketienziensis angulate*; Silicate taxa abbreviation: Eind-*Eunotia Indica*; Cbal-*Cyclotella baltica*; Clan – *Cymbella lanceolata*; Sneo – *Stephanodiscus neoastraea*; Csty – *Cyclotella stylorum*; Tfav –*Triceratium favus*; Acti – *Actinocyclus* spp.; Crad – *Cosinodiscus radiatus*; Cobs –*Coscinodiscus obscurus*; Aann – *Actinoptychus annulatus*; Cmar – *Coscinodiscus marginatus*; Pste – *Podosira stelliger*; Dfib – *Dictyocha fibula*; Cstr – *Cyclotella striata.*

with gravels (0.5–4 cm in diameter), locally (Fig. 2). No marine fossils were found. It is widely recognized as a fluvial deposit formed during the LGM when sea level was still on the continental shelf of the East China Sea (Li et al., 2000; Hori et al., 2001).

Unit II (63.8–49.7 m) is characterized by its grey to yellow thicker fine sand section. Brackish gastropod shells (whole and fragments), dominant species of foraminifera (*Ammonia beccarii* vars., and *A. convexidorsa*) and diatom (mainly *Cymbella lanceolata, Stephanodiscus neoastraea*, etc.) indicate a coastal water setting (Fig. 2). Three ^{14}C dates of this unit, ranging between ca. 12–10 ka, indicate the Early Holocene deposition (Fig. 2).

Unit III (49.7–38.7 m) differs from other units by its greyish clayey silt and silty clay. Dominant foraminifera (*A. beccarii* vars., *A. convexidorsa,* and *Epistominella naraensis*) and diatom (*Actinocyclus* spp.; *Cosinodiscus radiatus*; *C. obscurus*) indicate a more coastal water setting. Three ^{14}C dates ranging between ca. 10–9.0 ka indicate Early Holocene deposition.

Unit IV (38.7–22.9 m) is differentiated from other units by its yellowish–grey fine sand with a sharp sediment contact to the underlying sediment unit. Foraminifera are mainly *A. ketienziensis angulate* and *A. compressiuscula*, and diatom includes *Actinoptychus annulatus* and *Actinocyclus* spp. at the lower portion, but *C. marginatus, Podosira stelliger*, etc. at the upper section, meaning deeper estuarine water setting. Three ^{14}C dates, ranging between ca. 8.5–5.6 ka, indicate Early–Middle Holocene deposition.

Unit V (22.9–21.6 m) is composed mainly of greyish–yellow silty fine sand and clayey silt. Both foraminifera and diatom are of more coastal nature, represented by *A. beccarii* vars., *A. convexidorsa, A. pauciloculata, A. compressiuscula, Cyclotella baltica* and *Triceratium favus*. Although there is no ^{14}C date in this unit, it is inferred that this unit is of Middle Holocene age (Fig. 2).

Unit VI (21.2–4.0 m) is characterized by greyish silty sand and silt couplets. Foraminifera with coastal nature are represented by *A. beccarii* vars., *Florilus decorus* and *Bolivina robusta*, and diatom by *C. baltica* and *C. striata*. Three ^{14}C dates ranging between 3.1 and 2.1 ka indicate Late Holocene deposition.

Unit VII (4.0–0 m) has a fining–upward sediment sequence, in which rootlets and spotted Fe—Mn nodules were seen. Foraminifera are more coastal species, dominated by *A. beccarii* vars., *A. convexidorsa,* and *E. naraensis*, while diatom with similar water setting is represented by *Dictyocha fibula, Eunotia Indica* and *C. baltic*a. One ^{14}C date, ca. 1.7 ka, indicates Late Holocene deposition.

4.2. Sr, Ba and Sr/Ba

Sr and Ba are sensitive geochemical proxies for identification of saltwater and freshwater facies (Jaraula et al., 2014). The Sr/Ba ratio is particularly useful for the differentiation of sedimentary facies of brackish water origin (Wang et al., 2019). Sr/Ba in Unit I is generally between 1 and 3, the lowest in the core (Fig. 2). Sr/Ba of Unit II rises gradually to ca. 3–8. and to ca. 4–8 of Unit III. Sr/Ba further increases to ca. 7–11 of Unit IV (Fig. 2), the highest in core HM. Sr/Ba then gradually reduces to ca. 4–7 of Unit V, ca. 2–6 of Unit VI and ca. 2–4 of Unit VII. Sr/Ba of the present study helps define the completeness of Holocene strata and associated sedimentary environmental change of the valley with ecological implications being discussed below.

4.3. Sedimentation rate

The broader sedimentation rate of the Yangtze incised valley can refer Jiang et al. (2020). Here we focus HM core in context of 3 sections (Fig. 3). The highest sedimentation rate is in Unit I, the lowest sediment section of HM, with peak of 1.0 cm/y at ca. 12–8.5 ka (Fig. 3①). This is followed by a remarkably low rate of 0.1 cm/y occurring at ca. 8.5–4.5 ka (Fig. 3②). After this, a higher sedimentation rate of 0.7 cm/yr was observed in the core HM(Fig. 3③).

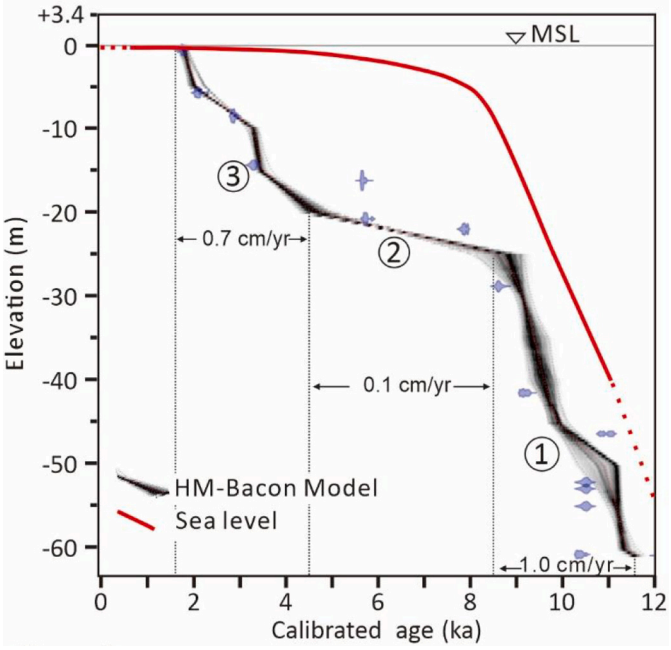

Fig. 3. Sedimentation rates for 3 sections of core HM determined by the BACON age–depth model (Seeing Fig. 2 for ^{14}C dates used) (Jiang et al., 2020) and the generalized Holocene sea-level curve of the Yangtze Delta (modified after Chen and Stanley, 1998; Hori et al., 2002; Zong, 2004).

4.4. Microfossil distribution

In total, 53 species of foraminifera and 60 diatom taxa were identified in core HM (S_Table 4, 5). In addition, one silicoflagellate (*D. fibula*) found in core samples was added to the microfossil database. No marine microfossils were found in the sediment of Unit I (69.8–63 m; Fig. 2).

Foraminifera were rare in the lower part of the core at depths of 63–22 m (ca. 12–5.0 ka). There was lower flux (D_{flux}) averaging 21 grains cm^{-2} yr^{-1}and species richness (D) of <2 (Fig. 4A and B). Only 14 grains cm^{-2} yr^{-1} and even <8 grains cm^{-2} yr^{-1} were found at the core depths 63–50 m and 38–22 m. Of note, a slightly higher foraminiferal flux of 40 grains cm^{-2} yr^{-1} occurred at 50–38 m. In contrast, foraminifera became significantly richer in the upper part of the core (22–0 m, ca. 5.0–0 ka), as shown by both D_{flux} increasing from 4 to 294 grains cm^{-2} yr^{-1} and D from 2 to 3.1 (Fig. 4A and B).

Most foraminiferal species in this study were benthic, with only a few planktonic (S_Table 4). The proportion of planktonic species showed an increasing trend (ca. 8–18%) after ca. 5.0 ka, in addition to somewhat higher values of 10–20% in the lower 50–38 m of the sediment section (Fig. 4C).

In contrast, diatoms were more abundant in the lower part of the core (63–32 m, ca. 12–9.0 ka), averaging 3 cells cm^{-2} yr^{-1} with a maximum of 7 × 10^4 cells cm^{-2} yr^{-1} with higher D (4–8.8) (Fig. 4D and E). However, D_{flux} above core depth 32 m (ca. 9.0 ka) became remarkably low (0.6 × 10^4 cells cm^{-2} yr^{-1}), and silicate taxa were absent in most samples (Fig. 4D).

The benthic diatom species are typically represented by *A. annulatus, C. nodulifer, C. argus, Achnanthes longipes, Brebissonia lanceolata, Biddulphia tuomegi, Cocconeis sublittoralis, Pleurosigma* spp. and *Eunotia* spp. The proportion of benthic diatoms remained low, seldom more than 5% before ca. 9.0 ka (Fig. 4F).

The silicate microalgae (diatom and silicoflagellate) can also be classified into freshwater, brackish and marine taxa according to their adaptation to salinity (Fig. 4G). The freshwater species remained at a relatively low proportion along core HM. Although the proportion of brackish water taxa varied within a limited range, the increasing trend of the brackish–marine group was apparent since ca. 9.0 ka as the

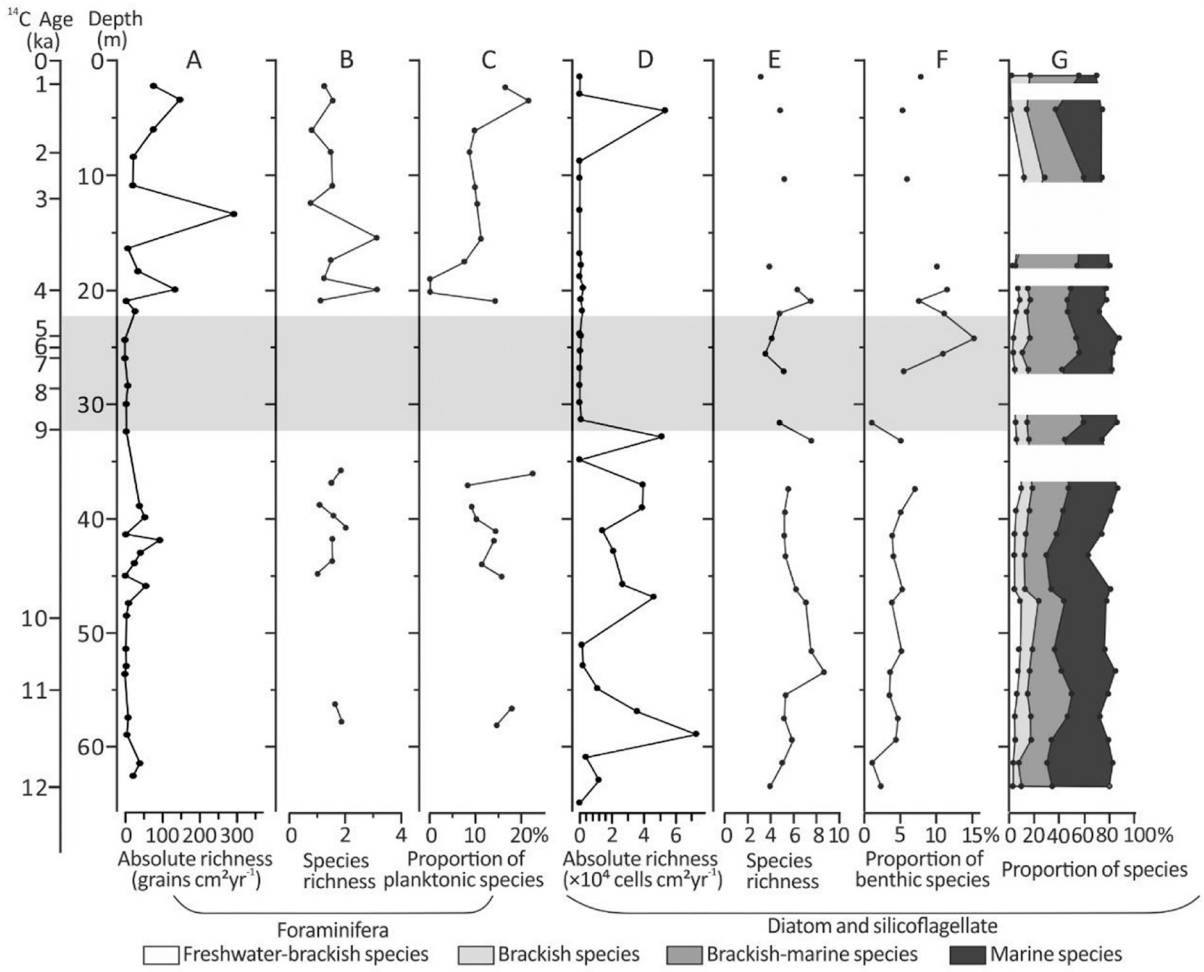

Fig. 4. Flux change of microfossils, species richness and proportions of specific taxa. The ages on the Y axis, expressed as ka, are based on the age–depth model in Fig. 3. The grey zone denotes low flux of both foraminifera and diatom.

marine species declined slightly.

A zone of low microfossil flux occurs at core depth 32–22 m (ca. 9.0–5.0 ka) (highlighted in GERY in Fig. 4). Of note, silicate microalgae diversity in this zone was somewhat higher (*D*: 3.6–5.2) (Fig. 4E).

4.5. Microfossil assemblages

The following analysis of the microfossil spectra of core HM is based only on the abundant microfossils of statistical significance, represented by the A–G assemblages in Fig. 4. The core section can be split at 22 m depth (ca 5.0 ka) where diatoms are richer below that level and foraminifera richer above. CONISS was used to help form the 4 (A–D) silicate assemblages at core depth 63–22 m, and the 3 (E–G) foraminiferal assemblages at 22–0 m as shown in Fig. 5.

Assemblage A (63–60 m, ca. 12–11 ka) is represented by diatom species including *Cymbella lanceolata* (brackish), *S. neoastraea* (freshwater/brackish), *Cyclotella stylorum* (brackish–marine) and *T. favus* (marine).

Assemblage B (60–40 m, ca. 11–9.5 ka) features mainly the marine species of *Actinocyclus* spp. (i.e. *A. normanii* and *A. ehrenbergii*), *C. radiatus*, and *C. obscurus*.

Assemblage C (40–32 m, ca.9.5–9.0 ka) consists mainly of marine species represented by *Actinocyclus* spp. However, the proportion of marine species decreases to some extent as shown by the lower numbers of *A. splendens, T. favus* and *C. radiatus* (Fig. 5). Here brackish water species *A. annulatus* increase to be included in this assemblage.

Assemblage D (32–22 m, ca. 9.0–5.0 ka) is a zone of fewer microfossils showing increasing brackish and brackish–marine species, represented by *C. marginatus, P. stelliger, D. fibula* and *C. striata*.

Assemblage E (22–18 m, ca. 4.5–3.8 ka) shows richer foraminifera represented by *A. beccarii* vars., *A. convexidorsa, A. pauciloculata* and *A. compressiuscula*.

Assemblage F (18–4 m, ca. 3.8–1.7 ka) is dominated by *A. beccarii* vars., *F. decorus, B. robusta;* and *B. marginate*.

Assemblage G (4–0 m, ca. 1.7–0 ka) is dominated by *A. beccarii* vars., *A. convexidorsa,* and *E.naraensis*.

5. Discussion

The Yangtze Delta serves as an immense sediment sink to accommodate a large amount of fluvial sediment from its huge catchment (1.80×10^6 km^2). The sediment was unevenly distributed in the Yangtze Delta, except the incised valley, where continuous sedimentation occurred at millennial scale during Holocene time (Wang et al., 2018; Jiang et al., 2020). The complete strata of HM, therefore, enables an improved understanding of the paleoenvironmental evolution of the Yangtze incised valley, in particular, as a sedimentary–ecological context.

5.1. Holocene environmental evolution: geo-bio-sedimentary proxies

The ^{14}C–dated HM covers the complete Holocene strata and

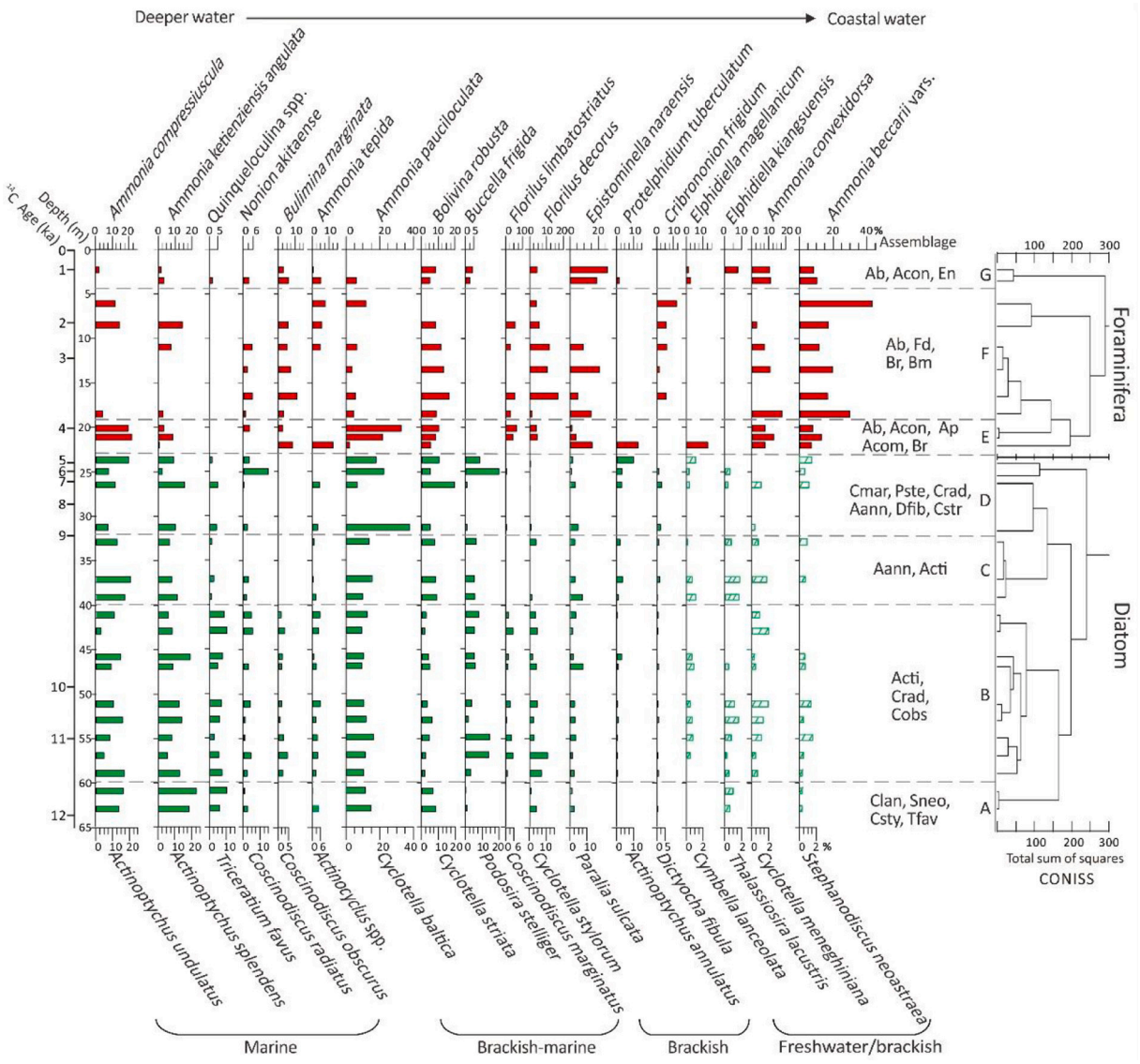

Fig. 5. Combined microfossil spectra of core HM (dominant species used); foraminifera and silicate taxa abbreviations refer Fig. 2.

associated environmental evolution, comprehended by the geo-bio-sedimentary proxies, (Fig. 2). Of note, Sr/Ba ratio in the brackish–marine facies of core HM, using the Sr/Ba–HAc method, is significantly higher (between ca. 3–11) (Fig. 2; S_Table 3) compared to 0.2–0.5 (brackish) and > 0.5 (marine) reported previously (Wei and Algeo, 2020). Given this, we do not use Sr/Ba to reconstruct paleosalinity in this study, since it must contain carbonate-hosted strontium from mother provenances (Wei and Algeo, 2020). Interestingly, the recent Sr/Ba measured from 3 Holocene sediment cores in the Yangtze incised valley using same method as this study demonstrated the similar trend in ratio through Holocene sedimentary facies (Chen et al., 2021). This convinces that Sr/Ba of HM can serve as a sedimentary facies indicator in relation to Holocene marine transgression and retrogression (Fig. 2).

In fact, Unit I-IV represents the Early-Middle Holocene marine transgressive processes (TST, Fig. 2). Prior to 12,000 years ago, the sea level of the study area was over 63 m below present (Unit I of Fig. 2). Shortly afterwards (ca. 12–10 ka), the valley was inundated by sea invasion. An increasing Sr/Ba (1–8) and the coastal foraminiferal/diatom assemblage in Unit II demonstrate a change to brackish water conditions (Fig. 2). As the sea level continued to rise, it led to the development of the estuarine facies (Unit III, 10–9.5 ka; Fig. 2) characterized by the further increasing Sr/Ba (3–8) and more coastal microfossils (Fig. 2). The estuarine conditions were further changed to the tidal sandy ridge facies ca. 9.5–5.5 ka (Unit IV, Fig. 2), which were widely developed in the study area (Hori et al., 2001). The peaking Sr/Ba (to 11) complies with the maximal Holocene marine transgression ca. 8000–7000 years ago (Jiang et al., 2020; Chen et al., 2021), supported by the deeper water foraminiferal/diatom assemblages (Fig. 2).

Unit V-VII represents the Middle-Late Holocene retrogressive deltaic processes (HST, Fig. 2). Deltaic sedimentation began ca. 5500 years ago with the prodelta and the delta front (Units V and VI), topped by the recent tidal flat facies (Unit VII). Decreased Sr/Ba (2–7), signified the brackish-coastal water setting at that time. Higher foraminiferal flux in these units consisting of dominant species of deeper to coastal water (Fig. 2) saw this environmental change.

Worldwide, prodelta deposition mainly began ca. 8000–7000 years ago, as deltaic formation occurred during the Holocene (Stanley and Warne, 1994). The belated occurrence of the prodelta facies at the core HM site ca. 5500 years ago was primarily due to the development of the sandy ridge facies in Unit IV, which was formed ca. 9500–5500 years ago (Fig. 2), a unique product of the strong in–out tidal sedimentation in the middle–outer incised valley (Li et al., 2000; Hori et al., 2001; Wang et al., 2018).

5.2. Sediment infilling pattern: 3 phases

5.2.1. Highest infilling phase: sourced from coastal sediments

The highest sedimentation rate in the valley of 1.0 cm/yr (Fig. 3①) can be ascribed to the large amplitude of sea-level rise in the Early Holocene (Hori et al., 2002; Jiang et al., 2020). This ca. 35-m sea-level rise created a huge flooded space in the incised valley for accommodating a great amount of sediment to infill (Figs. 2, 3), recorded as the thicker (>30 m) Early Holocene sediment in HM (Unit II–IV; Fig. 2). The rapid sedimentation in the Early Holocene, controlled by sea-level rise, has been seen in many incised valleys, such as the Mekong, where 19-m sediment was deposited in the period 9.0–8.0 ka (Ta et al., 2005).

The sediments of the Early Holocene that filled the valley were mainly thought to be brought from the adjacent coasts and the inner shelf during intensifying marine transgression, where there occurred mixtures of the older sediments both from the Yangtze River and

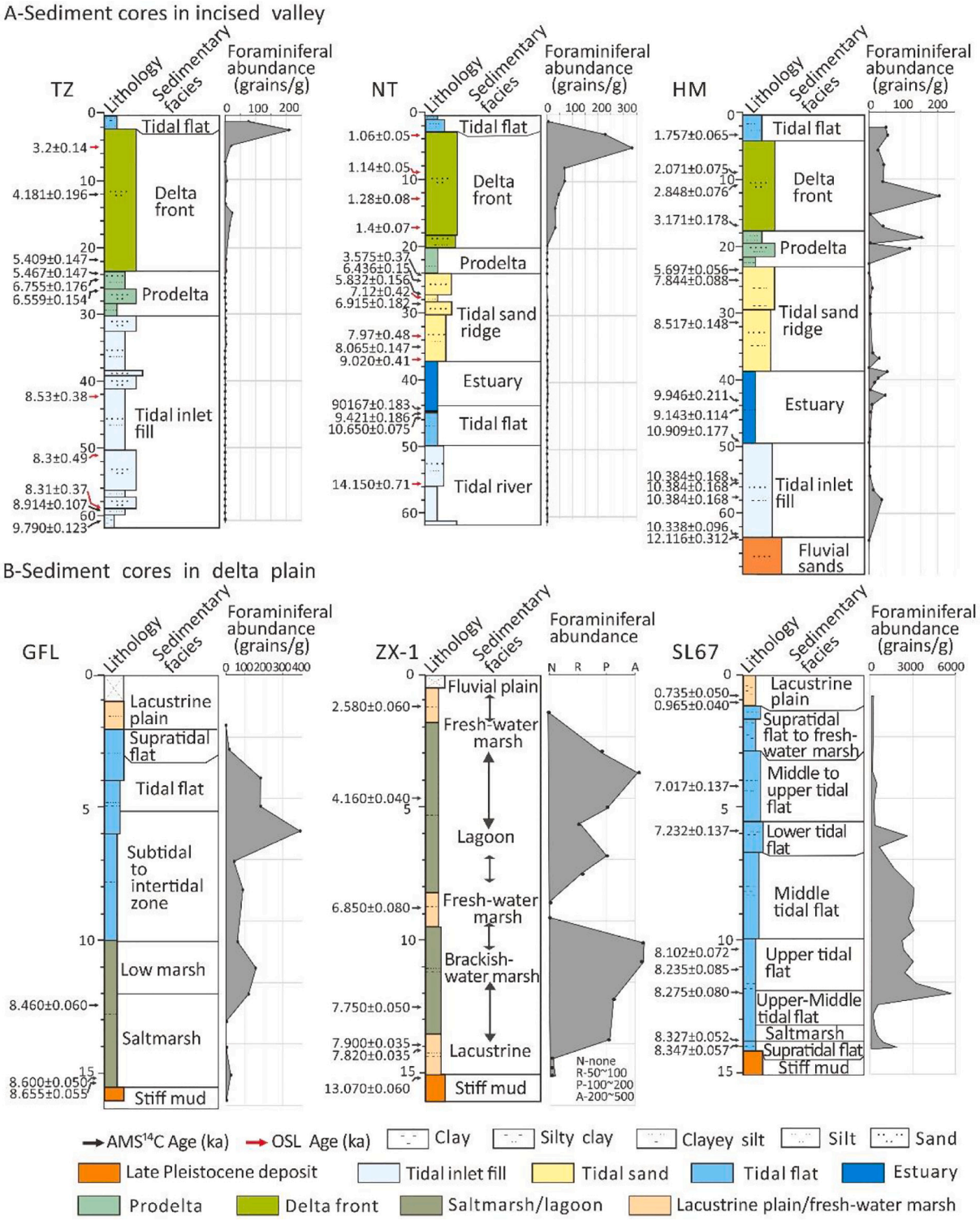

Fig. 6. Comparison of occurrences of foraminiferal distribution in the Holocene strata between the incised valley and the delta plain of the Yangtze Delta (core data of NT, GFL, ZX–1 and SL67 sourced from Chen et al., 2005; Wang et al., 2012, 2013; Jiang et al., 2020).

abandoned Yellow River (Chen et al., 2000; Liu et al., 2010), rather than directly from the river catchment. Ma (2017), using geochemical proxies, further proved that sediments in the Yangtze incised valley during the Early Holocene were transported partly from the East China continental shelf off the abandoned Yellow River coast to the north.

5.2.2. Fluvial infilling phase: sediment shortage in the mid–outer valley

There occurred a remarkably low sedimentation rate (0.1 cm/yr) in HM during ca. 8.5–4.5 ka (Fig. 3②). This is only 10% of the rate in the previous infilling phase with a similar time duration. Note that an even lower rate occurred in the outer incised valley, including the subaqueous delta, during this time period (Hori et al., 2001; Wang et al., 2010). Apparently, there was still space available in the valley caused by sea-level rise after ca. 8500 ka (Fig. 3). This means that ca. 8000–7000 years ago the depocenter was located at/or near the delta apex at Zhenjiang (Fig. 1A) when the sea had reached its maximum (Song et al., 2013; Jiang et al., 2020). Furthermore, sediment from the Yangtze River basin was insufficient to feed the HM core area in the mid–outer incised valley during 8.5–4.5 ka, a critical time given the ongoing debate about when sediment sourced from the Yangtze became sufficient to feed the southeast China coast during the Holocene (Liu et al., 2007; Xu et al., 2012; Gao, 2013). Our study highlights that the Yangtze sediment was not able to reach the distal coast before ca. 4.5 ka.

5.2.3. Depocenter shift seawards

After ca. 4.5 ka, a higher sedimentation rate of 0.7 cm/yr is seen in core HM (Fig. 3③) as shown by the 22 m thick deltaic sediments (Fig. 2), indicating rapid progradation and the seaward shift of the depocenter (Jiang et al., 2020).

5.3. Paleo–ecological implications

The unique ecological setting in the Yangtze incised valley can be primarily characterized by the lower to higher (both core–upward and seaward) foraminiferal distribution in the Holocene sediment cores HM, TZ and NT (Figs. 1, 6). Apparently, this is a reversal of the distribution pattern in cores GFL, ZX–1 and SL67 located on the delta plain (Figs. 1, 6).

The combined microfossil (foraminifera and diatom) spectra of core HM can shed further light on the paleo–ecological nature of the incised valley, in context of 3 stages of microfossil occurrences identified (Figs. 4, 5). The first, ca. 12–9.0 ka, consists of a remarkably low foraminiferal flux and numbers of species, but higher diatom flux and species. The second, ca. 9.0–5.0 ka, has fewer microfossils. The third stage, ca. 5.0–0 ka, has higher flux of foraminifera but fewer diatoms (Figs. 4, 5). The distinctive ecological implications of each stage are discussed below.

5.3.1. 12.0–9.0 ka: deeper valley with anoxic bottom water

This was the time when the incised valley had been inundated by the Early Holocene sea-level rise (>50 m; Fig. 3). The ecological conditions in the valley were affected by the rapid massive sediment accumulation of 1.0 cm/yr (Figs. 2, 3①). Given the sandy and muddy mixture in the Early Holocene (Fig. 2), presumably there was significantly higher sediment concentration in the seawater of the deeper valley, lowering the transparency of the bottom water. The anoxic deeper water (>60 m) of the valley had led to a lower primary productivity which suppressed the development of the benthic foraminiferal community (Fig. 4A, B; Niemistö et al., 2018). This is further confirmed by the lower proportion of benthic diatoms found in the Early Holocene sediment (Fig. 4F, Underwood and Kromkamp, 1999; Grinham et al., 2011). Pan's study (Pan, 2017) reported undeveloped foraminiferal communities in the Early Holocene sediment of the Yangtze incised valley. The taphonomic dissolution of benthic foraminifera of calcareous nature is another hypothesis that requires further study.

At the same time, richer diatoms and silicoflagellates provide evidence of higher productivity in the upper water body of the incised valley (Fig. 4D). The brackish–marine diatom communities in the Early Holocene sediments indicate a normal seawater body with sufficient transparency (Fig. 4D, E). The pattern of the diatom assemblage (A–D; Fig. 5) complies with the general trend of the Early–Middle Holocene sea-level rise.

The diatom assemblage A–B (12.0–9.5 ka) (Figs. 4, 5) contains freshwater–brackish (e.g. *S. neoastraea, C. lanceolata*) and marine species (*Actinocyclus* spp., *C. radiatus, C. obscurus*), consistent with the environmental change from coast to estuary in the Early Holocene (Figs. 2, 4, 5). Typical coastal species with lower halotolerance also appeared but seemed not to have survived well (Figs. 4, 5).

Also, the variation of species diversity (*D*: 4–8.8) of assemblage A–B, first rising and then slightly descending as water deepened in the incised valley, corresponds with the sea-level rise (Fig. 5E). The more brackish seawater may have maintained fewer species adapted to a hypersaline environment, reflecting the typical coastal to estuarine environmental change of the Early Holocene (Fig. 5).

In comparison, diatom assemblage C (ca. 9.5–9.0 ka; Fig. 5) contained a mixture of marine and brackish–marine taxa, represented by *Actinocyclus* spp., *A. annulatus, A. splendens*, and *T. favus* (>15%; Fig. 5). Here the paleo–environment of the incised valley contained more brackish water, favoring greater diversity of species (*D*: 4–6).

The transition to a more marine ecological setting took place at the HM core site in the mid–outer incised valley during the period ca. 11.6–9.5 ka, as indicated by the nature of the diatom community (Figs. 4, 5). Coincidently, there were sectional appearances of richness (*D*: 1–2) in the upper part of assemblage B (Fig. 4B), indicating a change from coastal to deeper estuarine water conditions during the Early Holocene sea-level rise.

5.3.2. ca. 9.0–5.0 ka: a time of poor bio–preservation

Foraminifera and diatom were rare in core HM during ca. 9.0–5.0 ka (Fig. 4). This coincided generally with the time of deposition of tidal sandy ridges that were a distinctive characteristics of the mid–outer incised valley (HM core site area; Fig. 2; Hori et al., 2001; Wang et al., 2018). The strong in–out tidal currents appear to have made the study area poorer for bio–preservation than any other places in the Yangtze Delta during that time as shown by cores GFL, ZX–1 and SL67 (Fig. 6). The somewhat higher richness of diatom (brackish–marine) species in assemblage D (Figs. 4, 5) hints at a change of ecological setting from marine to more coastal conditions during ca. 9.0–5.0 ka, when the sea-level rise decelerated towards the end of this stage (Chen et al., 2000; Zong, 2004).

5.3.3. ca. 5.0–0 ka: a salinity–reduced estuary favoring foraminifera but not diatom communities

This is the time of deltaic development after sea level had stabilized (Zong, 2004). The incised valley was nearly filled up with sediment and the water conditions favored the ecological development of the present estuary.

From the Assemblage E–G (Fig. 5), we can see the sensitive adaptation of foraminiferal communities to the changing ecological conditions in the Late Holocene (Figs. 4,5). The dominant species, including *A. beccarii* vars. and *A. convexidorsa*, were widely developed in the estuary (Assemblage E), which was then followed by the group of *F. decorus, B. robusta* and *B. marginate* (Assemblage F), showing a reduction in brackish tolerance during ca. 4.5–1.7 ka. Finally, the typical assemblage of *A. beccarii* vars., *A. convexidorsa,* and *E.naraensis* (Assemblage G) indicates the full establishment of coastal conditions. Interestingly, the slight increase in the proportion of planktonic species in the river mouth area since ca. 4.0 ka suggests a stronger influence of oceanic currents on the Yangtze coast (Fig. 4C).

Most benthic foraminifera examined in the present study were smaller in size and thinner than normal, primarily due to the lower salinity of the estuarine water, a result of the high discharge of the

Yangtze ($960 \times 10^{11} m^3 yr^{-1}$). It is evident that these benthic foraminifera had been gradually adapting to these estuarine conditions during the Late Holocene, but apparently the diatoms, dominated by brackish–marine species (Fig. 4G), followed a different trend, and were suppressed ecologically in these conditions of low salinity.

6. Conclusions

The large incised valley of the Yangtze Delta in which thicker and continuous Holocene sediment (>60 m) was deposited provides an invaluable sediment archive for the reconstruction of paleo–sedimentary–ecological complex. The complete Holocene strata of sediment core HM proved by Sr/Ba measurement were established as the TST and HST stratigraphic frameworks. The high sedimentation rate (1.0 cm/yr) occurred with coastal sediment filling into the valley driven by the Early Holocene marine transgression. It was then followed by the deltaic infilling with gradually increasing sedimentation rate, as the deltaic depocenter shifted seawards. Microfossil spectra is established and shows that the incised valley with a massive and rapid sediment infill in the Early Holocene was an unfavorable location for benthic foraminifera to develop, presumably in the low transparency bottom water. Nevertheless, at same time, diatom communities being as planktonic nature can flourish in the brackish water setting, which was replaced later by marine water as the sea level rose. The Middle Holocene tidal sandy ridge system prevailed in the mid–outer incised valley, making it a poorer location for microfossil preservation. Since then, foraminifera gradually became adapted to the reduced salinity of the estuarine water, but the diatoms did not as they were ecologically unsuited.

Supplementary data to this article can be found online at https://doi.org/10.1016/j.palaeo.2021.110387.

Declaration of Competing Interest

The authors declare that they have no known competing financial interests or personal relationships that could have appeared to influence the work reported in this paper.

Acknowledgements

We are grateful to Prof. W.G. Zhang and many graduate students of the State Key Laboratory of Estuarine and Coastal Research, East China Normal University, who helped generously with sediment coring and sediment logging. This study is financially supported by National Natural Science Foundation of China (Grant No. 41620104004; 41771226; 2016YFE0133700), and the Fundamental Research Funds for the Central Universities.

References

Battarbee, R.W., Jones, V.J., Flower, R.J., Cameron, N.G., Bennion, H., Carvalho, L., Juggins, S., 2001. Diatoms. In: Smol, J.P., Birks, H.J.B., Last, W.M., Bradley, R.S., Alverson, K. (Eds.), Tracking Environmental Change Using Lake Sediments. Kluwer Academic Publishers, Dordrecht, pp. 155–203.

Blaauw, M., Christen, J.A., 2011. Flexible paleoclimate age depth models using an autoregressive gamma process. Bayesian Anal. 6 (3), 457–474.

Blum, M., Martin, J., Milliken, K., Garvin, M., 2013. Paleovalley systems: insights from Quaternary analogs and experiments. Earth-Sci. Rev. 116, 128–169.

Boyd, R., Dalrymple, R.W., Zaitlin, B.A., Boyd, R.A., 2006. Estuarine and incised–valley facies models. In: Posamentier, H., Walker, R. (Eds.), Facies Models Revisited, SEPM Special Publication 84. Society for Sedimentary Geology, Tulsa, pp. 171–235.

Chaumillon, E., Tessier, B., Reynaud, J.Y., 2010. Stratigraphic records and variability of incised valleys and estuaries along French coasts. Bull. Soc. Géol. Fr. 181, 75–85.

Chen, Z., Stanley, D.J., 1998. Rising sea level on eastern China's Yangtze Delta. J. Coast. Res. 14 (1), 360–366.

Chen, J.Y., Shen, H.T., Yun, C.X., 1988. Morphodynamical Processes and Evolution of the Yangtze Estuary. Shanghai Scientific and Technological Press, 453pp (in Chinese).

Chen, Z.Y., Song, B.P., Wang, Z.H., Cai, Y.L., 2000. Late Quaternary evolution of the sub–aqueous Yangtze delta, China: sedimentation, stratigraphy, palynology, and deformation. Mar. Geol. 162, 423–441.

Chen, Z., Wang, Z., Schneiderman, J., Tao, J., Cai, Y., 2005. Holocene climate fluctuations in the Yangtze delta of eastern China and the Neolithic response. The Holocene 15 (6), 915–924.

Chen, Y., Zhang, W., Nian, X., Sun, Q., Ge, C., Hutchinson, S.M., Cheng, Q., Wang, F., Chen, J., Zhao, X.Q., 2021. Greigite as an indicator for salinity and sedimentation rate change: evidence from the Yangtze River Delta, China. J. Geophys. Res. Solid Earth 126, 1–16.

Clement, A.J.H., Fuller, I.C., 2018. Influence of system controls on the Late Quaternary geomorphic evolution of a rapidly–infilled incised–valley system: the lower Manawatu valley, North Island New Zealand. Geomorphology 303, 13–29.

Dalrymple, R.W., Zaitlin, B.A., Boyd, R.A., 1992. Estuarine facies models, conceptual basis and stratigraphic implications; discussion and reply. J. Sediment. Res. 64b, 74–77.

Dalrymple, R.W., Zaitlin, B.A., Boyd, R.A., 1994. Incised–Valley Systems: Origin and Sedimentary Sequences. In: SEPM, Special Publication, Vol. 51, 391p.

Gao, S., 2013. Holocene shelf–coastal sedimentary systems associated with the Changjiang River: an overview. Acta Oceanol. Sin. 32 (12), 4–12.

Greene, D.L., Rodriguez, A.B., Anderson, J.B., 2007. Seaward–branching coastal–plain and piedmont incised–valley systems through multiple sea–level cycles: Late Quaternary examples from Mobile Bay and Mississippi Sound, U.S.A. J. Sediment. Res. 77, 139–158.

Grimm, E.C., 1987. CONISS: a FORTRAN 77 program for stratigraphically constrained cluster analysis by the method of incremental sum of squares. Comput. Geosci. 13 (1), 13–35.

Grinham, A., Gale, D., Udy, J., 2011. Impact of sediment type, light and nutrient availability on benthic diatom communities of a large estuarine bay: Moreton Bay, Australia. J. Paleolimnol. 46 (4), 511–523.

Hill, M.O., Šmilauer, P., 2005. TWINSPAN for Windows version 2.3. Huntingdon. Centre for Ecology and Hydrology & University of South Bohemia, Ceske Budejovice.

Hori, K., Saito, Y., Zhao, Q., Cheng, X., Wang, P., Li, C., 2001. Sedimentary facies of the tide–dominated paleo–Changjiang (Yangtze) estuary during the last transgression. Mar. Geol. 177, 331–351.

Hori, K., Saito, Y., Zhao, Q., Cheng, X., Wang, P., 2002. Evolution of the coastal depositional system of the Changjiang (Yangtze) River in response to late Pleistocene–Holocene sea–level changes. J. Sediment. Res. 72, 884–897.

Jaraula, C.M.B., Siringan, F.P., Klingel, R., Sato, H., Yokoyama, Y., 2014. Records and causes of Holocene salinity shifts in Laguna de Bay, Philippines. Quat. Int. 349, 207–220.

Jiang, F., Zhao, X., Chen, J., Liu, Y., Sun, Q., Chen, J., Chen, Z., 2020. Depocenter shift and en–echelon shoal development in the pre–Holocene incised valley of the Yangtze Delta, China. Mar. Geol. 426, 106212.

Lei, Y.L., Li, T.G., 2016. Atlas of Benthic Foraminifera from China Seas. Science Press, Beijing, pp. 411.

Li, C., Chen, Q., Zhang, J., Yang, S., Fan, D., 2000. Stratigraphy and paleoenvironmental changes in the Yangtze Delta during the Late Quaternary. J. Asian Earth Sci. 18 (4), 453–469.

Li, C., Wang, P., Sun, H., Zhang, J., Fan, D., Deng, B., 2002. Late Quaternary incised–valley fill of the Yangtze delta (China): its stratigraphic framework and evolution. Sediment. Geol. 152, 133–158.

Liu, J.P., Xu, K.H., Li, A.C., Milliman, J.D., Velozzi, D.M., Xiao, S.B., Yang, Z.S., 2007. Flux and fate of Yangtze River sediment delivered to the East China Sea. Geomorphology 85, 208–224.

Liu, J., Saito, Y., Kong, X.H., Wang, H., Xiang, L.H., Wen, C., Nakashima, R., 2010. Sedimentary record of environmental evolution off the Yangtze River estuary, East China Sea, during the last w13,000 years, with special reference to the influence of the Yellow River on the Yangtze River delta during the last 600 years. Quat. Sci. Rev. 29, 2424–2438.

Ma, J., 2017. Study of Identification Source from the Yellow River in the Incised Yangtze Estuarine Valley and its Transport Mechanism during the Early to Mid–Holocene. MA dissertation. East China Normal University, pp. 1–67 (in Chinese with English abstract).

Margalef, R., 1968. Perspectives in Ecological Theory. University of Chicago Press, Chicago.

Niemistö, J., Kononets, M., Ekeroth, N., Tallberg, P., Tengberg, A., Hall, P.O.J., 2018. Benthic fluxes of oxygen and inorganic nutrients in the archipelago of Gulf of Finland Baltic Sea – effects of sediment resuspension measured in situ. J. Sea Res. 135, 95–106.

Pan, D., 2017. Migration of Land–Ocean Interaction Interface–Estuarine front in Holocene Sedimentary Record of the Yangtze River Mouth and its Mechanism. Ph.D Thesis. East China Normal University, pp. 1–176 (in Chinese with English abstract).

Pennington, B.T., Sturt, F., Wilson, P., Rowland, J., Brown, A.G., 2017. The fluvial evolution of the Holocene Nile Delta. Quat. Sci. Rev. 170, 212–231.

Pluet, J., Pirazzoli, P.A., 1991. World Atlas of Holocene Sea–Level Changes, Vol. 299. Elsevier Science.

Renberg, I., 1990. A procedure for preparing large sets of diatom slides from sediment cores. J. Paleolimnol. 4 (1), 87–90.

Song, B., Li, Z., Saito, Y., Okuno, J., Li, Z., Lu, A., Hua, D., Li, J., Li, Y., Nakashima, R., 2013. Initiation of the Changjiang (Yangtze) delta and its response to the mid–Holocene Sea level change. Palaeogeogr. Palaeoclimatol. Palaeoecol. 388, 81–97.

Stanley, D.J., Warne, A.G., 1994. Worldwide initiation of Holocene Marine Deltas by deceleration of sea–level rise. Science 265 (5169), 228–231.

Ta, T.K.O., Nguyen, V.L., Tateishi, M., Kobayashi, I., Saito, Y., 2005. Holocene delta evolution and depositional models of the Mekong River delta, southern Vietnam. In: Giosan, L., Bhattacharya, J. (Eds.), River Deltas—Concepts, Models, and Examples, Vol. 83. SEPM Spec. Publ., pp. 453–466

Tanabe, S., Saito, Y., Vu, L.Q., Hanebuth, T.J.J., Ngo, Q.L., Kitamura, A., 2006. Holocene evolution of the Song Hong (Red River) delta system, northern Vietnam. Sediment. Geol. 187, 29–61.
Tanabe, S., Nakanishi, T., Ishihara, Y., Nakashima, R., 2015. Millennial–scale stratigraphy of a tide–dominated incised valley during the last 14 kyr: spatial and quantitative reconstruction in the Tokyo Lowland, Central Japan. Sedimentology 62, 1837–1872.
Tjallingii, R., Stattegger, K., Wetzel, A., Phach, P.V., 2010. Infilling and flooding of the Mekong River incised–valley during deglacial sea–level rise. Quat. Sci. Rev. 29, 1432–1444.
Underwood, G.J.C., Kromkamp, J., 1999. Primary production by phytoplankton and microphytobenthos in estuaries. Adv. Ecol. Res. 29, 93–153.
Wang, P., Zhang, J., Min, Q., 1985. Distribution of foraminifera in surface sediments of the East China Sea. In: Marine Micropaleontology of China. Ocean Press, Beijing, pp. 34–69.
Wang, Z., Xu, H., Zhan, Q., Saito, Y., He, Z., Xie, J., Li, X., Dong, Y., 2010. Lithological and palynological evidence of late Quaternary depositional environments in the subaqueous Yangtze delta, China. Quat. Res. 73, 550–562.
Wang, Z., Zhuang, C., Saito, Y., Chen, J., Zhan, Q., Wang, X., 2012. Early mid–Holocene Sea–level change and coastal environmental response on the southern Yangtze delta plain, China: implications for the rise of Neolithic culture. Quat. Sci. Rev. 35, 51–62.
Wang, Z., Zhan, Q., Long, H., Saito, Y., Gao, X., Wu, X., Li, L., Zhao, Y., 2013. Early to mid–Holocene rapid sea–level rise and coastal response on the southern Yangtze delta plain, China. J. Quat. Sci. 28 (7), 659–672.
Wang, Z., Saito, Y., Zhan, Q., Nian, X., Pan, D., Wang, L., Chen, J., Xie, J., Li, X., Jiang, X., 2018. Three–dimensional evolution of the Yangtze River mouth, China during the Holocene: impacts of sea level, climate and human activity. Earth Sci. Rev. 185, 938–955.
Wang, A.H., Liu, J.K., Zhang, F., Huang, L., 2019. Selective extraction of sedimentogenic strontium and barium in terrigenous clastic sediments. In: United States Patent, No. US10151018 B2. 2018-12-11.
Wang, R., Colombera, L., Mountney, N.P., 2020. Quantitative analysis of the stratigraphic architecture of incised–valley fills: a global comparison of Quaternary systems. Earth Sci. Rev. 200, 102988.
Wei, W., Algeo, T.J., 2020. Elemental proxies for paleosalinity analysis of ancient shales and mudrocks. Geochim. Cosmochim. Acta 287, 341–366.
Xu, K., Li, A., Liu, J.P., Milliman, J.D., Yang, Z., Liu, C., Kao, S., Wang, S., Xu, F., 2012. Provenance, structure, and formation of the mud wedge along inner continental shelf of the East China Sea: a synthesis of the Yangtze dispersal system. Mar. Geol. 291–294, 176–191.
Yan, Q.S., Xu, S.Y., 1987. Recent Yangtze Delta Deposits. East China Normal University Press, Shanghai, pp 437 (in Chinese with English abstract).
Zaitlin, B.A., Dalrymple, R.W., Boyd, R., 1994. The stratigraphic organization of incised valley system. SEPM Spec. Publ. 51, 45–60.
Zong, Y.Q., 2004. Mid–Holocene Sea–level highstand along the Southeast Coast of China. Quat. Int. 117 (1), 55–67.